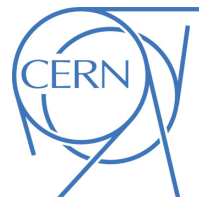




ATLAS NOTE

ATL-PHYS-PUB-2015-001

January 8, 2015



Performance and Calibration of the JetFitterCharm Algorithm for c-Jet Identification

The ATLAS Collaboration

Abstract

An impact parameter and secondary-vertex based charm tagging algorithm, JetFitterCharm, has been developed to distinguish c -quark jets from either b -quark or light-flavoured (u, d, s -quark or gluon) jets. JetFitterCharm is the first such algorithm used in ATLAS physics searches. This note presents both the expected performance in simulation and results from calibrating the tagging efficiencies of b -quark, c -quark and light-flavoured jets with data. The calibrations are presented in the form of scale factors, corresponding to the ratios of the tagging efficiencies measured in data to those in simulation. Both simulation and data are based on $\sqrt{s} = 8$ TeV pp collisions.



1 Introduction

Final states including c -jets can arise from a number of interesting processes at the Large Hadron Collider (LHC). Some of these, including Beyond the Standard Model $H \rightarrow c\bar{c}$ production [1] and SUSY models in which the lightest scalar quark decays to c -quarks [2], could be observed in LHC data. Unfortunately, in the absence of a designated c -quark jet (c -jet) identification algorithm, such searches are forced to contend with large Standard Model backgrounds: multijet production, b -quark jet (b -jet) backgrounds from $t\bar{t}$ decays, other electroweak processes, and $H \rightarrow b\bar{b}$ production can all overwhelm the c -jet signal. Even assuming that these backgrounds can be controlled using standard b -jet identification tools (b -tagging), these searches have little sensitivity to the jet flavour. To address these problems, a dedicated algorithm to identify c -jets (c -tagging) has been developed and applied to data collected by the ATLAS detector [3].

Flavour-tagging algorithms within ATLAS fall into two categories: those which identify b - and c -hadrons by their soft lepton decay products, and ‘lifetime-based’ methods which rely on the displacement of the b - and c -hadron decay products with respect to the primary vertex. The branching ratio of c -hadrons to leptons places an upper limit on the efficiency of soft-lepton based c -jet tagging algorithms, which restricts their usefulness for many analyses and as such has not been pursued further at this point. Lifetime-based methods are generally much more efficient and are well established in b -tagging, but so far the extension of these methods to c -tagging is less developed.

Lifetime-based tagging can be further divided into two general approaches. The first approach is based on the ‘impact parameter’ (IP) of tracks formed by charged particles in the inner tracking detector with respect to the primary interaction vertex. Impact parameter based tagging algorithms exploit the small IP generally associated to tracks within light-flavoured (u, d, s, gluon) jets (light-jets). Tracks from heavy hadron decays, by contrast, generally have a larger IP resulting from the displacement of the decay vertex. The second lifetime-based approach involves explicitly reconstructing at least one ‘secondary vertex’ (SV) from tracks within the jet and categorising the jet based on the SV properties.

A lifetime-based c -jet tagging algorithm must discriminate against two major backgrounds, b - and light-jets, and for most characteristics c -jets lie between these two extremes, making isolating them particularly challenging. In terms of light-jet discrimination, c -tagging algorithms are less powerful than b -tagging algorithms as a result of the smaller decay vertex displacement for c -hadrons relative to b -hadrons¹. This, combined with the effect of the lower D -hadron mass, results in smaller impact parameters and a lower SV reconstruction efficiency, and thus in a significantly lower c -tagging efficiency to reach a light-jet rejection equal to that achieved by b -tagging algorithms. On the other hand, it can be difficult to distinguish c -hadron candidates from b -hadrons because both can form a displaced SV and b -hadrons overwhelmingly decay via c -hadrons [4]. Faced with these complications, the best discriminating variables between b - and c -jets are the secondary vertex properties, in particular the invariant mass of the charged particles forming the secondary vertex.

Despite the limitations, lifetime-based c -tagging algorithms are within the capabilities of the detector and require only minor modifications to the existing b -tagging tools. This note describes the design of one such tagging algorithm, JetFitterCharm, and presents the expected performance and calibration on 2012 data. For Run 2 the additional new innermost pixel layer inserted into the ATLAS detector during 2014, denoted the Insertable B-Layer [5], is likely to further boost the c -tagging performance by significantly improving the impact parameter resolution for low momentum tracks.

¹The mean $c\tau$, where τ is the particle’s lifetime, for a B meson is $\approx 492 \mu\text{m}$, while $c\tau$ for a D^\pm (D^0) meson is only ≈ 312 (≈ 123) μm [4].

2 Data and Simulation Samples

All following performance plots are produced with $t\bar{t}$ events corresponding to 8 TeV proton-proton collisions simulated with POWHEG+PYTHIA6 [6, 7] and CT10 [8] parton distribution functions. Only $t\bar{t}$ decays with at least one lepton from a subsequent W decay are included. To simulate pileup, minimum bias interactions consistent with 2012 run conditions are generated with PYTHIA8 [9] and overlaid on the $t\bar{t}$ events. The propagation of particles through the detector and the detector response are modeled using GEANT4 [10]. The primary vertex is defined as the vertex with the largest sum of squared transverse momenta of the associated tracks.

Jets are reconstructed by clustering energy deposits in the calorimeter with the anti- k_t algorithm [11] and a radius parameter of 0.4, where clusters are calibrated with local cluster weighting [12]. Jet energy scale calibration and criteria to reject low quality jets are standard across most analyses of 2012 data, and are described in detail elsewhere [13]. In this note, only jets with transverse momentum, p_T , above 20 GeV and $|\eta| < 2.5$ are considered.² To mitigate effects from pileup, jets with $p_T < 50$ GeV and $|\eta| < 2.4$ are rejected if less than half of the sum of track p_T is associated with tracks matched to the primary vertex [14]. The same selection cuts are also applied for the data based calibrations presented in the second part of this document.

In the case of simulated jets, a flavour label is assigned by matching jets to generator level partons with $p_T > 5$ GeV, after final state radiation, in a $\Delta R < 0.3$ cone. If a b -quark is found within the cone the jet is labeled as a b -jet. If no b -quark is found, the search is repeated for c -quarks, then for τ leptons. If no match is found for b , c , or τ , the jet is labeled as a light-jet.

3 Algorithm

Within the ATLAS flavour-tagging framework algorithms are grouped into two classes: ‘basic tagging algorithms’, which convert detailed tracking information and jet kinematics into higher level variables relevant to flavour-tagging, and multivariate classifiers to combine these variables into a final discriminant. JetFitterCharm uses modified versions of the basic tagging algorithms and combines these with a neural network to produce a set of c -tagging discriminants.

3.1 Basic Tagging Algorithms

Tracks are selected within a ΔR cone surrounding the jet center in the calorimeter, which varies as a function of the transverse momentum of the jet [15]. These tracks are then passed to three basic tagging algorithms, which distill the available information into 19 variables per jet. These algorithms are summarised briefly below, while a more detailed description can be found in Ref. [15].

IP3D: The IP3D tagging algorithm takes as inputs the transverse and longitudinal signed impact parameter significance of tracks with respect to the primary vertex, S_{xy} and S_z . Based on these a two-dimensional likelihood function is computed from simulation, separately for b and light jet flavours. The IP3D outputs, \mathcal{L}_b and $\mathcal{L}_{\text{light}}$ are then calculated according to $\mathcal{L}_f = \prod_{k=0}^{N_{\text{tracks}}} \mathcal{L}_f^{\text{trk}}(S_{xy,k}, S_{z,k})$ where the f subscripts represent the two flavours of jet and \mathcal{L}^{trk} is the likelihood function derived from simulation.³

²ATLAS uses a coordinate system with its origin at the nominal interaction point (IP) in the center of the detector and the z -axis along the beam pipe. Cylindrical coordinates (r, ϕ) are used in the transverse plane, ϕ being the azimuthal angle around the beam pipe. The pseudorapidity is defined in terms of the polar angle θ as $\eta = -\ln \tan(\theta/2)$, while $\Delta R \equiv (\Delta\eta^2 + \Delta\phi^2)^{1/2}$.

³A likelihood function for c -jets has since been added to IP3D, but wasn’t available when JetFitterCharm was finalised.

SV1: SV1 reconstructs secondary vertex candidates by first forming ‘two-track’ vertices from pairs of tracks. It then removes vertices compatible with photon conversions, K_0 and Λ decays, or which are likely to originate from hadronic interactions with the beampipe and inner pixel layers. As a final step, it clusters all tracks associated to remaining two-track vertices into a single secondary vertex candidate [16]. Various secondary vertex properties, as detailed in Table 1, are calculated from all the associated tracks. These properties are among the best discriminants between c - and b -jets.

JetFitter: JetFitter attempts to reconstruct the b - to c -hadron decay chain under the hypothesis that the primary, b - and c -hadron vertices are approximately aligned on a single ‘flight line’ [17]. The flight line is initialised beginning at the reconstructed primary vertex and extending along the direction of the jet axis. This flight line is then iteratively updated while ‘single-track vertices’ are fit by constraining tracks to intersect the flight line within the uncertainty of their trajectories. JetFitter then merges clusters of single-track vertices, while further updating the flight line, to form a well-defined decay chain consisting of multi-track and single-track vertices. Many properties of the decay chain are useful as jet-flavour discriminants. These properties (listed in Table 1) offer complementary information with respect to SV1.

The JetFitter algorithm relies on a number of tuned parameters which specify which tracks are considered and how vertices are formed. To resolve more secondary vertices in c -jets, JetFitter-Charm uses a retuned variant of this algorithm in which the track selection is loosened, tracks are less likely to be assigned to the primary vertex, and single track vertices are more likely to be formed near the primary vertex. In addition several variables are added to the JetFitter outputs: transverse displacement of the secondary and tertiary vertices (L_{xy}^1 and L_{xy}^2), and the track rapidity along the jet axis, $\varphi_{\text{trk}} \equiv \tan^{-1} \mathbf{p}_{\text{trk}} \cdot \hat{\mathbf{p}}_{\text{jet}} / E_{\text{trk}}$.

3.2 Neural Network

Variables summarised in Table 1 are passed into a neural network, which consists of 4 layers: one input layer with 19 input nodes, two hidden layers with 20 and 10 nodes respectively, and three output nodes. The three output nodes correspond to the posterior probability that a jet is b , c , or light flavoured, and are referred to as P_b , P_c , and P_{light} respectively.

The network was trained on b -, c - and light-jets selected from simulated $t\bar{t}$ events. The interpretation of the neural network outputs as posterior probabilities depends upon the prior flavour composition of the training sample. Training begins by initialising the synapse weights and node activation thresholds with random values. The classification error $E \equiv \sum_f (T_f - P_f)^2$, where $f \in \{b, c, \text{light}\}$ and T_f are target posteriors, is then minimised with the backpropagation algorithm as implemented in the JETNET [18] package. Target posteriors are assigned according to the labeling scheme described in Section 2: the target value T_f is defined to be one if f matches the jet flavour label and zero otherwise. As a precaution against training the neural network with a kinematic flavour bias, the training sample is reweighed in two-dimensional categories of p_T^{cat} and η^{cat} , such that the relative fractions of b -, c - and light-jets are constant in all categories. In this training scheme, the target posteriors sum to one in each jet by definition, whereas the P_f values would sum to one only in the limit of perfect training, and in reality show a deviation from one at the percent level.

Algorithm	Variable Name	Description
Kinematic	p_T^{cat}	p_T category of jet, divisions [GeV]: 15, 25, 35, 50, 80, 120, 200, ∞
	η^{cat}	$ \eta $ category of jet, divisions: 0, 0.7, 1.5, 2.5
IP3D	$\log(\mathcal{L}_b/\mathcal{L}_{\text{light}})$	log ratio between b -jet and light-jet likelihood value
SV1	$n_{\text{trk}}^{\text{SV1}}$	Number of tracks matched to the vertex
	n_{2t}	Number of two-track vertices found in the jet
	m_{vx}	Secondary vertex mass
	L/σ_L	Secondary vertex flight-length significance
JetFitter	m_{chain}	Invariant mass of decay products
	S_d^{JF}	Total vertex flight-length significance
	n_{vx}	Number of reconstructed vertices with ≥ 2 tracks
	$n_{\text{trk}}^{\text{JF}}$	Number of tracks matched to vertices with ≥ 2 tracks
	n_{1t}	Number of single-track vertices
	L_{xy}^1	Transverse displacement of the secondary vertex
	L_{xy}^2	Transverse displacement of the tertiary vertex
	$\min \varphi_{\text{trk}}$	Minimum track rapidity along jet axis
	$\langle \varphi_{\text{trk}} \rangle$	Mean track rapidity along jet axis
	$\max \varphi_{\text{trk}}$	Maximum track rapidity along jet axis
SV1, JetFitter (variables input from both)	$E_{\text{vx}}/E_{\text{jet}}$	Ratio of the vertex track energy sum to the jet track energy sum

Table 1: Summary of the variables used by the JetFitterCharm neural network. JetFitterCharm uses a ‘charm tuned’ variant of the standard JetFitter used by other ATLAS tagging algorithms. The charm tuned JetFitter also adds the variables L_{xy}^1 , L_{xy}^2 , and φ_{trk} . Note that φ_{trk} is the track rapidity computed with respect to the jet axis. The total significance of JetFitter vertices is computed as $S_d^{\text{JF}} = (\sum_i L_i/\sigma_i^2)/(\sum_i 1/\sigma_i^2)^{1/2}$, where i indexes the tracks, L is the vertex displacement, and σ is the vertex displacement uncertainty.

4 Operating Points

The three posterior probabilities produced by the neural network, sum to approximately 1 and thus contain one redundant degree of freedom. The three outputs are therefore projected into a 2-dimensional ‘anti- b ’ versus ‘anti-light’ discriminant plane as shown in Fig. 1, where the anti- b axis is defined as $\log(P_c/P_b)$ and the anti-light axis as $\log(P_c/P_{\text{light}})$; both variables are shown in Fig. 2. Operating points are defined by a pair of minimum thresholds: any jet in which both the anti-light and anti- b discriminants exceed the thresholds is said to be ‘tagged’.

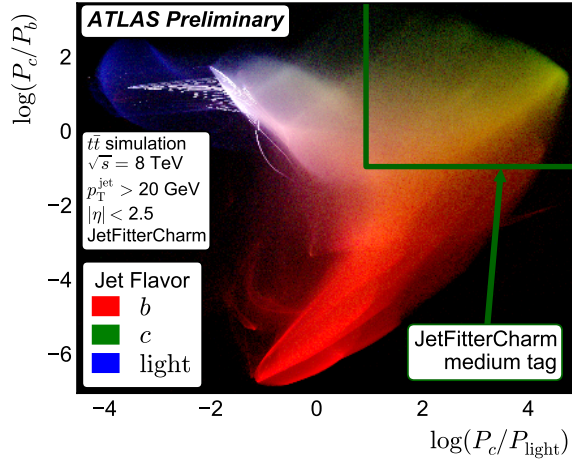


Figure 1: Two-dimensional distribution of the JetFitterCharm anti- b ($\log(P_c/P_b)$) and anti-light ($\log(P_c/P_{\text{light}})$) discriminants. The density of red, green, and blue reflect the density of b , c , and light jets, white areas are a mix of all three flavours, whereas black areas lack any jets. The ‘medium’ calibrated operating point selects jets above a certain threshold in both anti- b and anti-light discriminants. Ridge structures arise from two features of the algorithm which concentrate values in the input space. The first feature is the use of discrete kinematic bin inputs, η^{cat} and $p_{\text{T}}^{\text{cat}}$. The second is the substitution of default values when the ordinary input values would not be physically meaningful, for example when no secondary vertex is found. The resulting high density structures can be seen in the lower-center and upper-left region of the plot.

Charm tagging, being relatively new to the LHC, is unable to draw on extensive past experience in physics analyses to define ideal operating points. The operating points were therefore defined with a SUSY \tilde{t} pair production search [2] as a prototype. In this particular model, the \tilde{t} quarks decay via $\tilde{t} \rightarrow c \tilde{\chi}_1^0$, leading to a final state with two c -jets. Before applying c -tagging, expected signal events contribute to the signal region at the percent level, while top backgrounds contribute roughly 10% and the remaining events are split evenly between W and Z production in association with jets. The leading four jets were considered for tagging. The anti- b and anti-light tagging thresholds were allowed to vary independently of each other while maximising the expected signal significance. This procedure was repeated to produce four candidate operating points for each of several dozen mass combinations in the $m_{\tilde{t}}-m_{\tilde{\chi}_1^0}$ plane.

These studies demonstrated that many candidate operating points can be collapsed into two operating points without significant loss of performance. For cases where light jet backgrounds dominate, a ‘medium’ tag is defined to reject both light- and b -flavoured jets. In other selections light jets are a

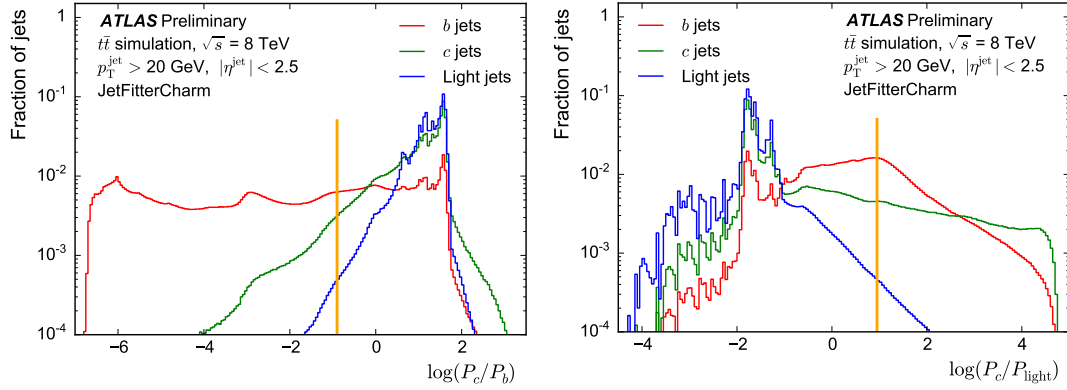


Figure 2: Distributions of the JetFitterCharm anti-bottom (left) and anti-light (right) discriminants. The total numbers of jets of each flavour has been normalised to 1. Minimum thresholds for tagged jets are indicated by orange vertical lines. A loose tag requires an anti-bottom discriminant above the threshold, whereas a medium tag requires both anti-bottom and anti-light discriminants above the indicated thresholds.

smaller background and $t\bar{t}$ becomes dominant, so a second ‘loose’ tag is defined which rejects over half of b jets while accepting a larger fraction of c -jets. These operating points are summarised in Table 2.

Operating Point	$\log(P_c/P_b)$	$\log(P_c/P_{\text{light}})$	ϵ_c	$1/\epsilon_b$	$1/\epsilon_{\text{light}}$
Loose	> -0.9	–	0.95	2.5	1.0
Medium	> -0.9	> 0.95	0.20	8.0	200

Table 2: c -tagging operating points. Charm tagging requires two cuts: one to reject b jets, and another to reject light jets. The approximate efficiency for c jets along with the rejection for b and light jets, with $p_T > 20$ GeV and $|\eta| < 2.5$ as estimated on $t\bar{t}$ events, are also given.

5 Performance

The c -tagging efficiencies as a function of p_T and $|\eta|$ for the medium and loose operating points are shown in Fig. 3.

Beyond the two currently calibrated operating points, many more combinations of anti- b and anti-light thresholds could be useful, depending on a number of analysis-dependent factors such as the number of tags applied and the flavour composition of the dominant backgrounds. The range of possible operating points is illustrated in two ways. The first, shown on the left of Fig. 4, gives the light-jet rejection as a function of c -jet efficiency for all possible values of the anti-light threshold (x -axis in Fig. 1). In this case, the anti- b threshold is adjusted to maintain a constant b -jet rejection. Similar information is given on the right side of Fig. 4 in the form of c -jet constant efficiency contours in the light- versus b -jet rejection plane. Both figures demonstrate the trade off between b -jet and light-jet rejection: for example for constant 30% c -tagging efficiency an operating point can double its b -jet rejection at the expense of cutting the light-jet rejection by a factor of 10.

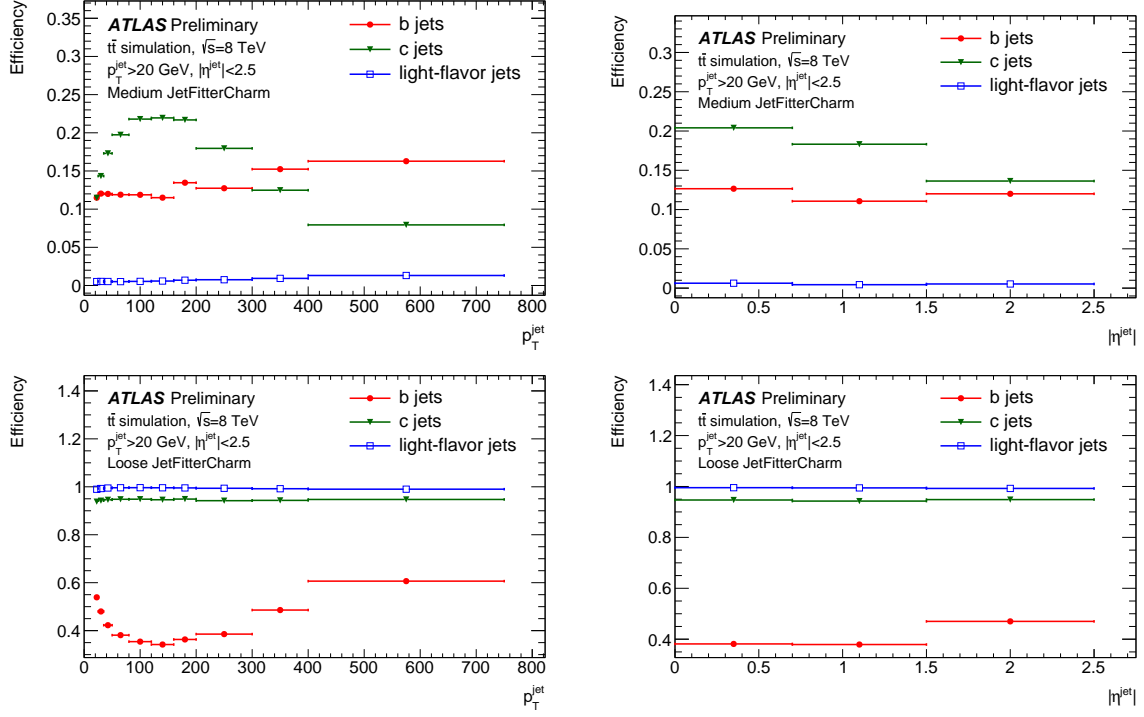


Figure 3: Dependence of the tagging efficiencies on the jet transverse momentum (left) or pseudorapidity (right) for b -, c -, and light-flavour jets for the JetFitterCharm medium (top) and loose (bottom) operating points. The medium and loose operating points were chosen to give an average c -tagging efficiency of $\approx 20\%$ and $\approx 95\%$. The jets are from $t\bar{t}$ simulated events generated with POWHEG+PYTHIA6.

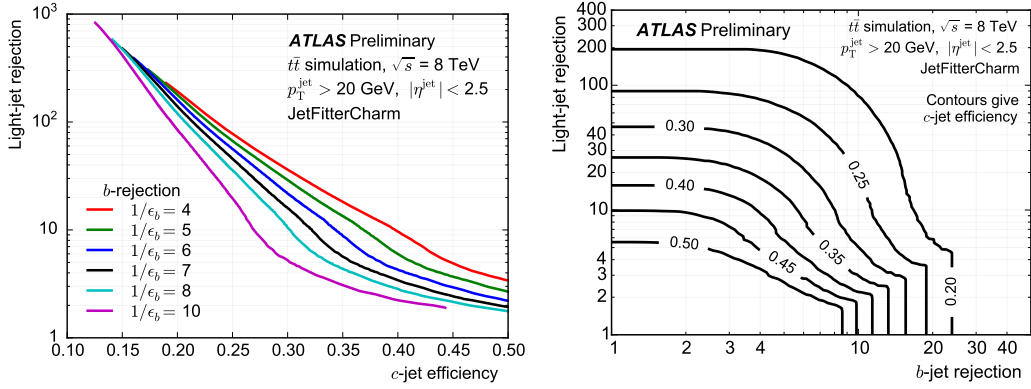


Figure 4: JetFitterCharm light-jet rejection versus c -tagging efficiency, where the b -rejection ($1/\epsilon_b$) is held fixed (left). Bottom rejection versus light rejection for constant charm-tagging efficiency (right). JetFitterCharm operating points select jets above a pair of thresholds in a 2-dimensional discriminant plane, thus for any c -tagging efficiency a range of b and light rejections are possible.

6 Calibration

Separate analyses are used to calibrate each of the three jet flavours. The efficiency for tagging b -jets is determined from a measurement performed in dileptonic $t\bar{t}$ events with two or three jets, and is based on a combinatorial likelihood approach [19]. The c -jet tagging efficiency has been calibrated in multijet events where jets contain D^* mesons [20]. Light-jet scale factors are derived from a negative-tag analysis [20]. All three calibrations are performed as a function of jet transverse momentum and are provided in terms of scale factors, defined as the ratio of the tagging efficiencies measured in data to those predicted by simulation. Light-jet scale factors are further binned as a function of $|\eta|$. No η -binning is used for b - and c -jet scale factors, as these scale factors have no significant dependence on jet η . Figures 5 and 6 give scale factors for all jets at the medium operating point. Figures 7 and 8 give the same information for the loose operating point.

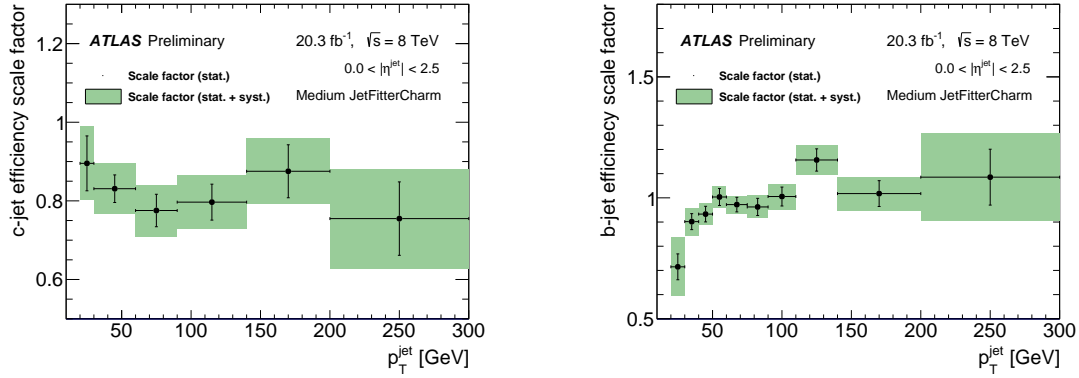


Figure 5: Dependence of the c -jet (left) and b -jet (right) efficiency scale factors on the jet transverse momentum for the medium operating point of the JetFitterCharm tagging algorithm. The derivation of the b -tagging (c -tagging) scale factors, shown here relative to $t\bar{t}$ Powheg+Pythia6 (dijet Pythia8), is detailed in [19] ([20]).

7 Conclusions

Dedicated c -jet tagging algorithms provide a new tool to isolate final states containing c -jets from light and b -jet related backgrounds, whilst also improving the sensitivity to the flavour composition. JetFitterCharm, the first generation set of such tagging algorithms in ATLAS, combines established b -tagging tools to produce a flexible set of c -tagging discriminants. With these discriminants a range of operating points can be defined, several of which have now been calibrated on the 2012 $\sqrt{s} = 8 \text{ TeV}$ dataset. The calibrations are provided in terms of scale factors with their systematic and statistical uncertainties, allowing dedicated c -tagging algorithms to be used in ATLAS analyses for the first time.

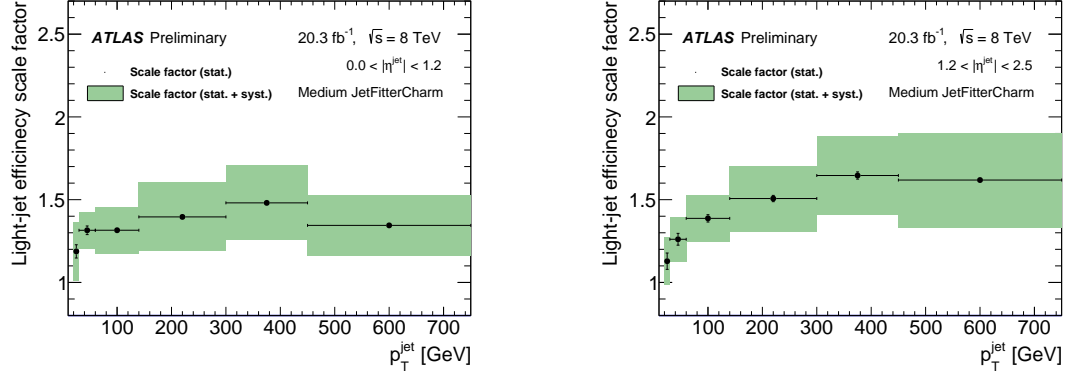


Figure 6: Dependence of the light-jet efficiency scale factor on the jet transverse momentum, for jet pseudorapidity $0.0 < |\eta| < 1.2$ (left) and $1.2 < |\eta| < 2.5$ (right), for the medium operating point of the JetFitterCharm tagging algorithm, as detailed in [20]. The scale factors are measured relative to dijet Pythia8+EvtGen.

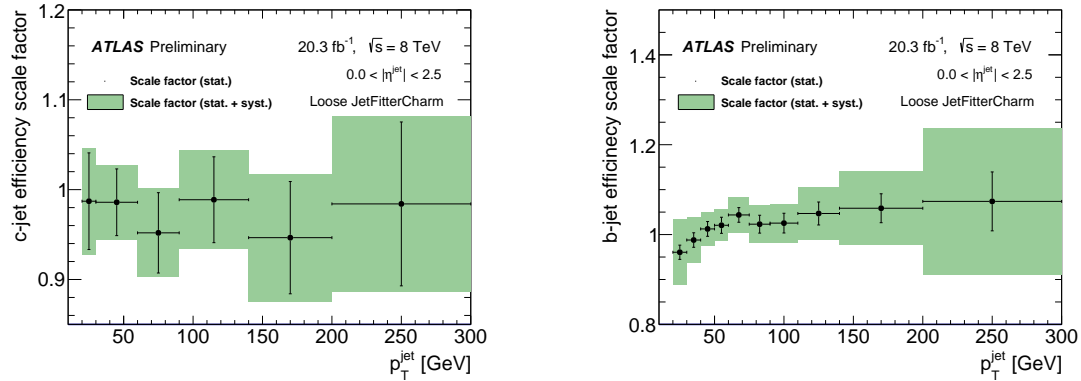


Figure 7: Dependence of the c -jet (left) and b -jet (right) efficiency scale factors on the jet transverse momentum for the loose operating point of the JetFitterCharm tagging algorithm. The derivation of the b -tagging (c -tagging) scale factors, shown here relative to $t\bar{t}$ Powheg+Pythia6 (dijet Pythia8), is detailed in [19] ([20]).

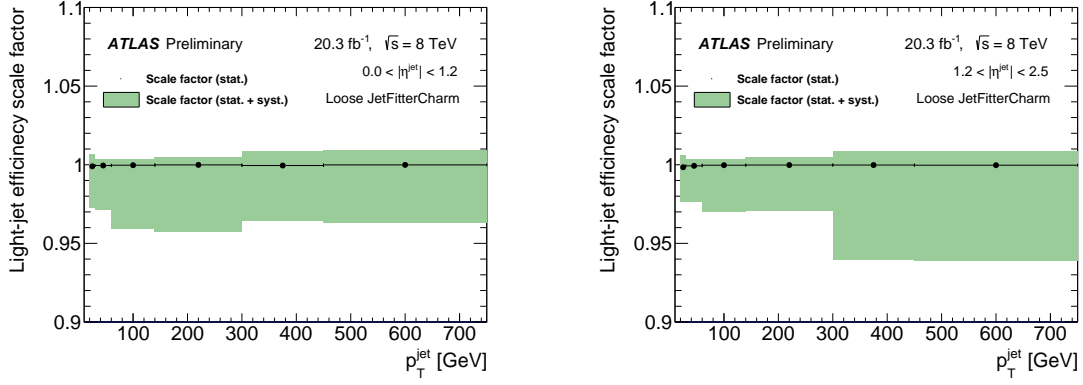


Figure 8: Dependence of the light-jet efficiency scale factor on the jet transverse momentum, for jet pseudorapidity $0.0 < |\eta| < 1.2$ (left) and $1.2 < |\eta| < 2.5$ (right), for the loose operating point of the JetFitterCharm tagging algorithm, as detailed in [20]. The scale factors are measured relative to dijet Pythia8+EvtGen. The total uncertainty is constrained to give a maximum corrected efficiency of 1.

References

- [1] C. Delaunay, T. Golling, G. Perez, and Y. Soreq, *Enhanced Higgs boson coupling to charm pairs*, *Phys. Rev. D* **89** (2014) 033014.
- [2] ATLAS Collaboration, *Search for pair-produced third-generation squarks decaying via charm quarks or in compressed supersymmetric scenarios in pp collisions at $\sqrt{s} = 8$ TeV with the ATLAS detector*, *Phys. Rev. D* **90** (2014) 052008, [arXiv:1407.0608 \[hep-ex\]](#).
- [3] ATLAS Collaboration, *The ATLAS Experiment at the CERN Large Hadron Collider*, JINST **3** (2008) S08003.
- [4] Particle Data Group Collaboration, K. A. Olive and others, *Review of Particle Physics*, *Chin. Phys. C* **38** (2014) 090001.
- [5] ATLAS Collaboration, *ATLAS Insertable B-Layer Technical Design Report*, Tech. Rep. CERN-LHCC-2010-013. ATLAS-TDR-19, CERN, Geneva, Sep, 2010. <https://cds.cern.ch/record/1291633>.
- [6] P. Nason, *A new method for combining NLO QCD with shower Monte Carlo algorithms*, JHEP **11** (2004) 040, [arXiv:0409146 \[hep-ph\]](#).
- [7] T. Sjöstrand, S. Mrenna, and P. Z. Skands, *PYTHIA 6.4 Physics and Manual*, JHEP **05** (2006) 026.
- [8] H. L. Lai et al., *New parton distributions for collider physics*, *Phys.Rev. D* **82** (2010), [arXiv:1007.2241 \[hep-ph\]](#).
- [9] T. Sjöstrand, S. Mrenna, and P. Z. Skands, *A Brief Introduction to PYTHIA 8.1*, *Comput.Phys.Commun.* **178** (2008) 852–867, [arXiv:0710.3820 \[hep-ph\]](#).
- [10] GEANT4 Collaboration, S. Agostinelli et al., *GEANT4: A simulation toolkit*, *Nucl. Instrum. Meth. A* **506** (2003) 250–303. <http://geant4.web.cern.ch/geant4/>.
- [11] M. Cacciari, G. P. Salam, and G. Soyez, *The anti- k_t jet clustering algorithm*, JHEP **04** (2008) 063, [arXiv:0802.1189 \[hep-ph\]](#).
- [12] ATLAS Collaboration, T. Barillari et al., *Local hadronic calibration*, ATL-LARG-PUB-2009-001-2. <https://cds.cern.ch/record/1112035>.
- [13] ATLAS Collaboration, *Jet energy measurement with the ATLAS detector in proton- proton collisions at $\sqrt{s} = 7$ TeV*, *Eur. Phys. J. C* **73** (2013) 2304, [arXiv:1112.6426 \[hep-ex\]](#).
- [14] ATLAS Collaboration, *Pile-up subtraction and suppression for jets in ATLAS*, ATLAS-CONF-2013-08, <https://cds.cern.ch/record/1570994>.
- [15] ATLAS Collaboration, *Commissioning of high performance b -tagging algorithms with the ATLAS detector*, ATLAS-CONF-2011-102. <http://cdsweb.cern.ch/record/1369219>.
- [16] ATLAS Collaboration, *Performance of the ATLAS Secondary Vertex b -tagging Algorithm in 7 TeV Collision Data*, ATLAS-CONF-2010-042. <http://cdsweb.cern.ch/record/1277682>.

- [17] G. Piacquadio and C. Weiser, *A new inclusive secondary vertex algorithm for b-jet tagging in ATLAS*, *J. Phys. Conf. Ser.* **119** (2008) 032032.
- [18] C. Peterson, T. Rognvaldsson, and L. Lonnblad, *JETNET 3.0: A Versatile artificial neural network package*, *Comput. Phys. Commun.* **81** (1994) 185–220.
- [19] ATLAS Collaboration, *Calibration of b-tagging using dileptonic top pair events in a combinatorial likelihood approach with the ATLAS experiment*, ATLAS-CONF-2014-004.
<http://cdsweb.cern.ch/record/1664335>.
- [20] ATLAS Collaboration, *Calibration of the performance of b-tagging for c and light-flavour jets in the 2012 ATLAS data*, ATLAS-CONF-2014-046.
<http://cdsweb.cern.ch/record/1741020>.